

Optical strong coupling in hybrid metal-graphene metamaterial for terahertz sensing

Ling Xu(徐玲), Yun Shen(沈云), Liangliang Gu(顾亮亮), Yin Li(李寅), Xiaohua Deng(邓晓华), Zhifu Wei(魏之傅), Jianwei Xu(徐建伟), and Juncheng Cao(曹俊诚)

Citation: Chin. Phys. B, 2021, 30 (**11**): 118702. DOI: 10.1088/1674-1056/abfb58

Journal homepage: http://cpb.iphy.ac.cn; http://iopscience.iop.org/cpb

What follows is a list of articles you may be interested in

A new viewpoint and model of neural signal generation and transmission: Signal transmission on myelinated neuron

Zuoxian Xiang(向左鲜), Chuanxiang Tang(唐传祥), Lixin Yan(颜立新), Chao Chang(常超)†, and Guozhi Liu(刘国治)‡

Chin. Phys. B, 2020, 29 (**10**): 108701. DOI: 10.1088/1674-1056/abaee9

Terahertz polarization conversion and sensing with double-layer chiral metasurface

Zi-Yang Zhang(张子扬), Fei Fan(范飞), Teng-Fei Li(李腾飞), Yun-Yun Ji(冀允允), Sheng-Jiang Chang(常胜江)

Chin. Phys. B, 2020, 29 (**7**): 078707. DOI: 10.1088/1674-1056/ab9294

Polarization conversion metasurface in terahertz region

Chen Zhou(周晨), Jiu-Sheng Li(李九生)

Chin. Phys. B, 2020, 29 (**7**): 078706. DOI: 10.1088/1674-1056/ab9295

Broadband terahertz time-domain spectroscopy and fast FMCW imaging: Principle and applications

Yao-Chun Shen(沈耀春), Xing-Yu Yang(杨星宇), Zi-Jian Zhang(张子健)

Chin. Phys. B, 2020, 29 (**7**): 078705. DOI: 10.1088/1674-1056/ab9296

Terahertz coherent detection via two-color laser pulses of various frequency ratios

Xin-Yang Gu(顾新杨), Ke-Jia Wang(王可嘉), Zhen-Gang Yang(杨振刚), Jin-Song Liu(刘劲松)

Chin. Phys. B, 2019, 28 (**9**): 098701. DOI: 10.1088/1674-1056/ab37fc

---

Optical strong coupling in hybrid metal-graphene metamaterial for terahertz sensing*

Ling Xu(徐玲)[1], Yun Shen(沈云)[1,†], Liangliang Gu(顾亮亮)[2], Yin Li(李寅)[1], Xiaohua Deng(邓晓华)[3], Zhifu Wei(魏之傅)[1], Jianwei Xu(徐建伟)[1], and Juncheng Cao(曹俊诚)[4]

[1] *Department of Physics, Nanchang University, Nanchang* 330031, *China*
[2] *School of Optical-Electrical and Computer Engineering, University of Shanghai for Science and Technology, Shanghai* 200093, *China*
[3] *Institute of Space Science and Technology, Nanchang University, Nanchang* 330031, *China*
[4] *Shanghai Institute of Microsystem and Information, Chinese Academy of Sciences, Shanghai* 200050, *China*

(Received 4 February 2021; revised manuscript received 20 March 2021; accepted manuscript online 26 April 2021)

We propose a terahertz hybrid metamaterial composed of subwavelength metallic slits and graphene plasmonic ribbons for sensing application. This special design can cause the interaction between the plasmon resonances of the metallic slits and graphene ribbons, giving rise to a strong coupling effect and Rabi splitting. Intricate balancing in the strong coupling region can be perturbed by the carrier concentration of graphene, which is subject to the analyte on its surface. Thereby, the detection of analyte can be reflected as a frequency shift of resonance in terahertz transmission spectra. The result shows that this sensor can achieve a theoretical detection limit of 325 electrons or holes per square micrometer. Meanwhile, it also works well as a refractive index sensor with the frequency sensitivity of 485 GHz/RIU. Our results may contribute to design of ultra-micro terahertz sensors.

Keywords: metamaterial, terahertz, strong coupling, sensor

PACS: 87.50.U–, 87.85.fk **DOI:** 10.1088/1674-1056/abfb58

1. Introduction

Graphene has potential to reshape landscape of chemical and biomolecules sensors owing to its good biocompatibility and tunable surface chemistry.[1,2] It can strongly enhance light-matter interactions at a deeply sub-wavelength size scale when graphene is operated as an optical resonator, due to the ability to support surface plasmons with extremely high confinement. Most importantly, graphene plasmons can be tuned via doping. This advantage gives rise to highly sensitive detection of some molecules which can alter charge carriers of graphene by absorbing on surface of graphene.[3] So far, various targeting analytes such as glucose,[4] protein,[5] nucleic acids,[6] pesticides[7] and bacterial[8] have been qualitatively or quantitatively determined by graphene sensors.

Recently, graphene-based hybrid metamaterials were proposed to further enhance light–matter interactions and improve sensitivity of systems.[9,10] In hybrid metamaterials, strong coupling between two different resonant modes of subsystems allows excitation of hybrid polariton modes, leading to further near-field localization and enhancement in comparison with either resonant mode alone. Such modification in spectroscopic response of two new normal modes is known as the vacuum Rabi splitting.[11,12] As the electric field localization and enhancement can hopefully offer potential applications including tunable optical switches,[13] multiband absorbers,[14] and high sensitivity sensors,[15] couplings in graphene-based metamaterials deserve further study.

In this work, aiming at an ultra-micro THz sensing, we propose a novel sensor model involving strong coupling between extraordinary optical transmission (EOT) in subwavelength metallic slits and graphene surface plasmons (GSPs) in graphene ribbons. It shows a good performance on detection of target molecules which perturb the carrier concentration of graphene by acting as donors or acceptors. Because of the high sensitivity of graphene to molecular doping and the high sensitivity of intricate balancing between EOT and GSPs modes in the strong coupling, the detection limit of target molecules based on this sensor can be as low as 325 electrons or holes per square micrometer.

2. Design and mechanism

The setup of our proposed hybrid metamaterial sensor is schematically illustrated in Fig. 1(a). It functionally involves three main parts: (i) the subwavelength metallic slits inspiring EOT, (ii) the embedded graphene plasmonic ribbons supporting GSPs, and (iii) the transparent polyimide (PI) substrate with low permittivity. In the hybrid metamaterials, strong coupling between EOT and GSPs allows the excitation of hybrid polariton modes, which can be modeled by diagonalizing the Hamiltonian of the coupled system[16] as follows:

$$H = \begin{bmatrix} \omega_{\mathrm{EOT}} - \mathrm{i}\gamma_{\mathrm{EOT}} & g \\ g & \omega_{\mathrm{GSPs}} + \omega' - \mathrm{i}\gamma_{\mathrm{GSPs}} \end{bmatrix}. \quad (1)$$

*Project supported by the National Natural Science Foundation of China (Grant Nos. 61865009, 61927813, and 62005168).
†Corresponding author. E-mail: shenyun@ncu.edu.cn
© 2021 Chinese Physical Society and IOP Publishing Ltd

Here, ω_{EOT} and ω_{GSPs} denote the resonances of the EOT and the GSPs, respectively; $\omega' = \omega_{\mathrm{EOT}} - \omega_{\mathrm{GSPs}}$ is the detuning between EOT and GSPs resonance frequencies and denotes the frequency shift of GSPs caused by external perturbation; γ_{EOT} is the decay rates of EOT; γ_{GSPs} is the decay rate of GSPs and inversely proportional to relaxation time τ, i.e., $\gamma_{\mathrm{GSPs}} = 1/2\tau$; g denotes coupling strength. Furthermore, the eigen-frequencies of Eq. (1) can be obtained as

$$\omega_{\pm} = \frac{\omega_{\mathrm{EOT}} + \omega_{\mathrm{GSPs}}}{2} \pm \mathrm{Re}\left[\sqrt{\frac{1}{4}\left(\omega' - \mathrm{i}\left(\gamma_{\mathrm{EOT}} - \gamma_{\mathrm{GSPs}}\right)\right)^2 + g^2}\right]. \quad (2)$$

Equations (1) and (2) demonstrate that coupling between resonant modes of ω_{EOT} and ω_{GSPs} allows the excitation of new hybrid polariton modes $\omega_{\pm}$. The $\Omega = (\omega_+ - \omega_-)$ is defined as Rabi frequency, which reflects the rate of energy exchange between EOT mode and GSPs mode.

To realize the strong coupling and Rabi splitting, geometrical parameters in the proposed structure of Fig. 1(a) are set as $p = 150$ μm, $a = 90$ μm, $b = 60$ μm, $w = 10$ μm, and $h = 47$ μm. The substrate is PI with permittivity $\varepsilon_{\mathrm{d}} = 3.2(1 + \mathrm{i}0.02)$ and subwavelength metallic slits are Au with conductivity $\sigma_{\mathrm{Au}} = 4.09 \times 10^7$ S/m. These geometric parameters have already been optimized in preliminary test. In THz wavelength ranges, it has been proven that the optical response of graphene is dominated by intraband transitions rather than interband transitions. Thus, the conductivity of graphene (σ_{g}) is simplified to a Drude-like model:[17]

$$\sigma_{\mathrm{g}} = \frac{\mathrm{i}e^2}{\pi\hbar^2}\frac{E_{\mathrm{F}}}{\omega + \mathrm{i}\tau^{-1}},$$

and carrier concentration can be deduced by $n = (|E_{\mathrm{F}}|/\hbar\upsilon_{\mathrm{F}})^2/\pi$. Here e is electron charge, $\hbar$ is reduced Planck constant, E_{F} is Fermi energy, ω is angular frequency, and $\upsilon_{\mathrm{F}} = 1.1 \times 10^6$ m/s is the Fermi velocity in graphene. Additionally, the carrier relaxation time is defined as $\tau = \mu E_{\mathrm{F}}/e\upsilon_{\mathrm{F}}$. In our study, the simulation is performed by computer simulation technology (CST). Specifically, the graphene monolayer in the simulation is modeled as a material with thickness $t_{\mathrm{g}} = 0.34$ nm and an equivalent relative permittivity $\varepsilon_{\mathrm{g}} = 1 + \mathrm{i}\sigma_{\mathrm{g}}/\varepsilon\omega t_{\mathrm{g}}$.[18] Here σ_{g} is determined by τ and carrier concentration n, which is artificially set in the simulation; and ε_0 is permittivity of vacuum space.

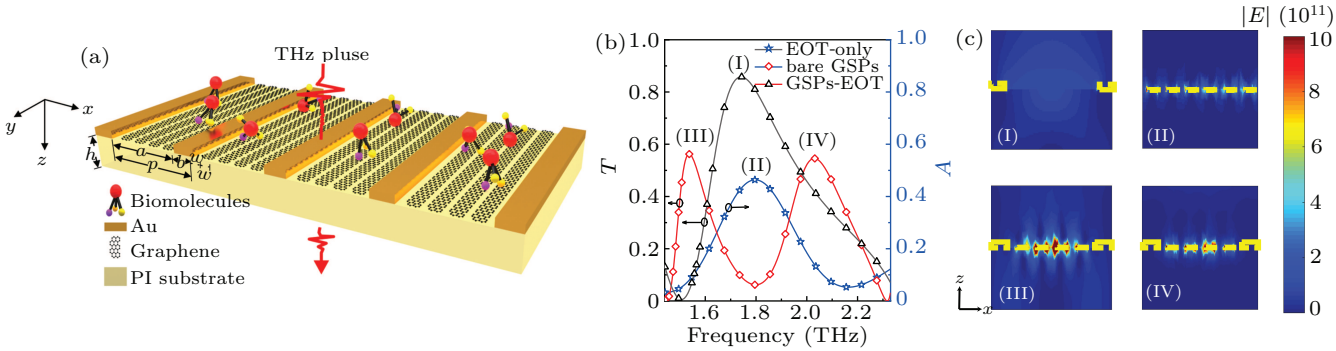


Fig. 1. (a) Schematic of the proposed hybrid metal-graphene metamaterial. The geometrical parameters are $p = 150$ μm, $a = 90$ μm, $b = 60$ μm, $w = 10$ μm, and $h = 47$ μm, respectively. (b) Optical response of the subwavelength metallic slits (blue line), bare graphene ribbons (blue line), and hybrid metamaterial (red curve) with carrier relaxation time τ and carrier concentration n of graphene are 1 ps and 2.4×10^4 μm^{-2}, respectively. (c) I–IV are the distributions of total electric field ($|E|$) at peak points in curves I–IV of (b), respectively.

To figure out the functionality of the various components, we first established the optical response of the subwavelength metallic slits. In Fig. 1(b), the gray curve shows the transmission spectrum of metallic slits. The EOT resonance frequency at $f = 1.75$ THz (point I) is determined by the subwavelength metallic slit array period. Secondly, we adopted graphene ribbons with 10 μm/20 μm of width/period. The blue curve in Fig. 1(b) represents the absorption spectrum of GSPs. The absorbance of GSPs reaches 0.5 at 1.79 THz (point Ⅱ). Here, relaxation time τ and carrier concentration n of graphene are severally set as 1 ps and 2.4×10^4 μm^{-2}. Considered to the coupling strength depends on the ratio of the quality factor of the cavity to the mode volume, we optimized the substrate thickness to maximize the strength of electric field located around graphene. According to Fabry–Pérot resonance, the thickness of PI is set as 47 μm. Finally, the graphene ribbons are embedded into metal grating slits to form hybrid metamaterials, the Rabi splitting response are shown in Fig. 1(b) by the red curve. It is shown that there appear two resonances peaks at $\omega_- = 1.53$ THz (point Ⅲ) and $\omega_+ = 2.02$ THz (point Ⅳ). In this case, $\Omega = 0.49$ THz and $\Omega/\omega_{\mathrm{EOT}} > 10\%$ are obtained, indicating that strong coupling of EOT and GSPs modes takes place.[19] It is noted that the results in Fig. 1(b) well verify the model of Eqs. (1) and (2), which demonstrate that coupling between resonant modes ω_{EOT} and ω_{GSPs} allows the excitation of new hybrid polariton modes $\omega_{\pm}$. The distributions of electric field ($|E|$) at peak points in curves I–IV in Fig. 1(b) are shown by pictures I–IV in Fig. 1(c), respectively. Figure 1(c)(I) demonstrate that fields of EOT resonance mainly localize within the gap of slits. Figure 1(c)(Ⅱ) illustrates that

fields of GSPs resonance localize in the vicinity of graphene ribbons. As seen in Fig. 1(c) [(Ⅲ) and (Ⅳ)] demonstrating fields of two new Rabi splitting modes ω_+ and ω_-, we can see that both the electric fields of ω_+ and ω_- are much stronger than those in I and Ⅱ, implying that hybrid metamaterial can provide further field enhancement in comparison with either resonant mode alone and lead to high sensitivity of system.

3. Results and discussion

Owing to the high carrier mobility and atomic thickness, graphene shows an ultra-high sensitivity to doping perturbations from the external environment.[20] Many molecules with electron withdrawing or donating groups on the graphene surface can lead to p- and n-type doping of graphene, respectively. This gives rise to the change of carrier concentration of graphene,[21] which appears as the variation in Rabi splitting. To study the performance of the proposed graphene-based hybrid metamaterials as a sensor, we first simulated the evolution of the Rabi splitting with the carrier concentration of graphene. As shown in Fig. 2(a), the position of splitting peaks shows a redshift/blueshift when carrier concentration is below/above 2.4×10^4 μm^{-2}. We note that the splitting will disappear and be out of sensing range as n is less than 1.4×10^4 μm^{-2} or greater than 6.2×10^4 μm^{-2} because the coupling becomes much weaker. Figure 2(b) shows the transmittance map of the coupling between EOT and GSPs as a function of frequency and carrier densities. From Fig. 2(b) we can see that the two hybrid modes of Rabi splitting are separated by a gap instead of crossing to each other.

The sensitivity of the hybrid system can be assessed by examining the variations of the Rabi frequency Ω and dip point frequency $f_{\rm dip}$ at the transmission spectral versus carrier concentration n, defined as $S_\Omega=\Delta\Omega/\Delta n$ and $S_{\rm dip}=\Delta f_{\rm dip}/\Delta n$, respectively. The dependence of Ω and $f_{\rm dip}$ on n are extracted and depicted in Figs. 3(a) and 3(b) marked with red points, respectively. The slopes of fitting lines in Figs. 3(a) and 3(b) are $S_\Omega=7\times10^{-6}$ THz/μm^2 and $S_{\rm dip}=1.54\times10^{-5}$ THz/μm^2.

In practice, the sensor resolution is defined as $R=R_{\rm instr}/S_{\Omega,{\rm dip}}$, where $R_{\rm instr}$ is instrumental resolution determined by noise level at the sensor output. Here, $R_{\rm instr}$ refers to the frequency resolution of time-domain terahertz spectrometer and is usually equivalent to 5 GHz.[22] Thus, $R_\Omega=714$ μm^{-2} and $R_{\rm dip}=325$ μm^{-2} can be achieved, respectively. This means that the proposed metal-graphene hybrid system in Fig. 1(a) can effectively detect analytes which change carrier concentration n of graphene more than 325 carriers per μm^2 through withdrawing or donating groups on graphene surface.

Next, the effect of relaxation time τ of graphene on the properties of the hybrid system are investigated. Figure 4(a) shows the Rabi splitting transmission for different τ of graphene as carrier concentration $n=2.4\times10^4$ μm^{-2}. The phenomenon of Rabi splitting becomes more obvious with the increaseing τ, indicating that lower loss provides better Rabi splitting. In addition, the $f_{\rm dip}$ has a subtle variation. Specifically, the variations of $f_{\rm dip}$ versus n for different τ are shown in Fig. 4(b). For all τ, $f_{\rm dip}$ increases linearly as n increases. Then, slopes of the curves, which are $S_{\rm dip}=\Delta f_{\rm dip}/\Delta n$ and indicate system's sensitivities, are also calculated and illustrated in Fig. 4(c). The turning point can be observed at about 0.6 ps, and $S_{\rm dip}$ gradually becomes flat after 0.6 ps.

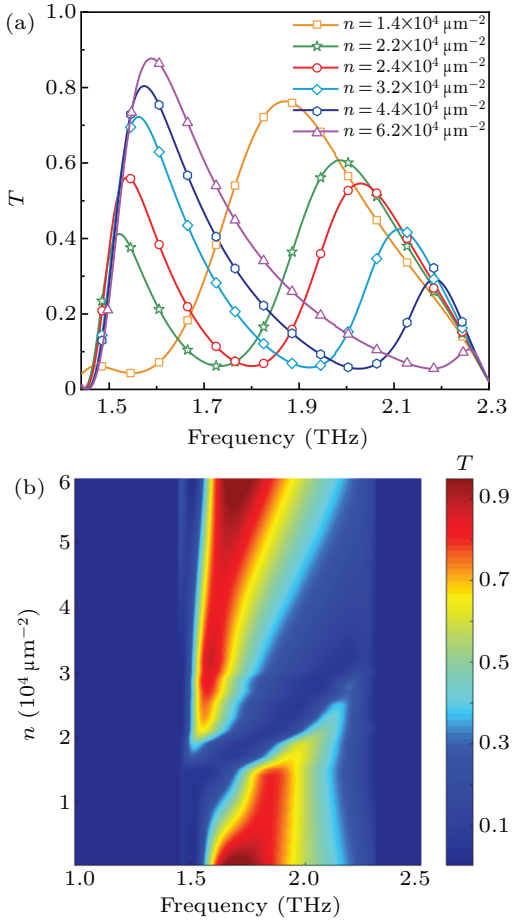


Fig. 2. (a) Transmission spectra of hybrid metal-graphene metamaterials with carrier concentration ranging from 1.4×10^4 μm^{-2} to 6.2×10^4 μm^{-2}. (b) Transmittance map exhibiting graphene plasmon (GSPs) absorption and extraordinary optical transmission (EOT) as a function of frequency and graphene carrier concentration n.

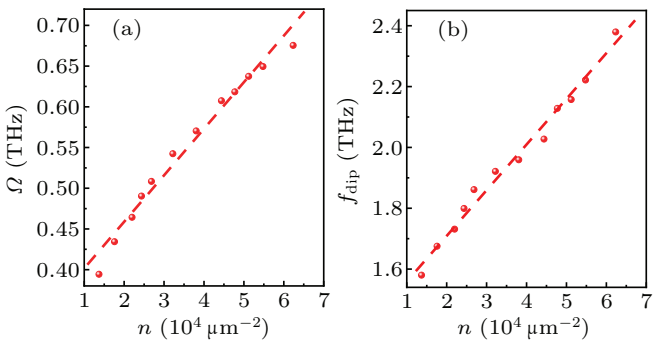


Fig. 3. The dependence of (a) Ω and (b) $f_{\rm dip}$ on carrier concentration n. The points are the simulation data and fitted by the dashed lines.

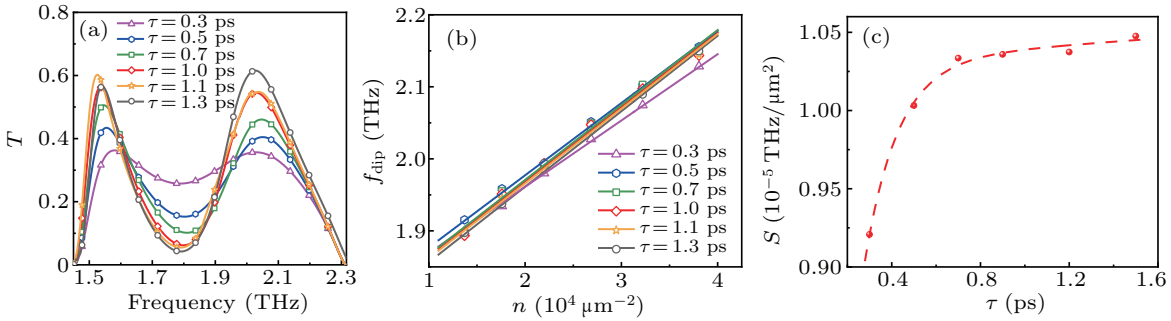


Fig. 4. (a) Rabi splitting transmission for different relaxation time τ of graphene as carrier concentration $n = 2.4 \times 10^4$ μm^{-2}. (b) Variations of $f_{\rm dip}$ versus n for different τ. (c) Sensitivity $S_{\rm dip}$ versus τ.

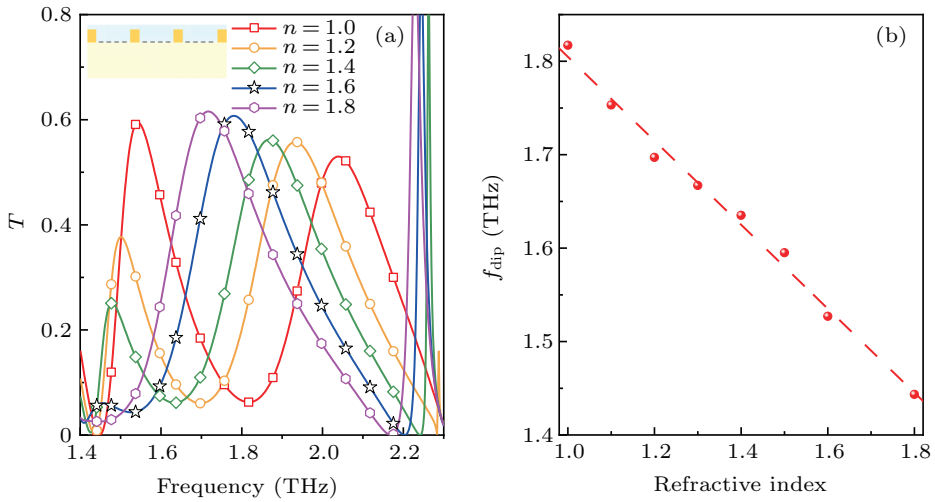


Fig. 5. (a) Transmission spectra of the proposed hybrid-metamaterial working as refractive index sensor. (b) Dip frequency variations versus different analyte refractive indices.

Additionally, our sensor can work well as a refractive index sensor. To verify this, one analyte layer with a thickness of 6 μm on the sensor surface is depicted in the inset of Fig. 5(a). The curves in Fig. 5(a) reveal the dependence of the transmission spectrum on the analyte refractive index in the range of 1.0–1.8, corresponding to the common biomolecules like DNA and RNA.[23] The refractive index sensitivity is obtained as 485 GHz/RIU from the fitting line in Fig. 5(b). This is much higher than the traditional refractive index sensors reported previously.[24,25] The advantage of our sensor is ascribed to the strong confinement of the electromagnetic fields realized by the strong coupling. Nevertheless, compared to the sensitivity based on the doping sensing mechanism, much larger amount of analyte is required to result in the change of THz response when it works as a refractive index sensor.[26,27] Thus, sensing by doping of graphene is the greatest advantage of our system.

4. Conclusion

In conclusion, we have proposed an ultra-micro THz sensor based on the strong coupling resonance via the interference between EOT and GSPs. The analyte adsorbed on the surface of graphene leads to a variation of the carrier concentration of graphene because of charge transfer process, further result in a variation in Rabi splitting. The simulation result shows that the detection limit of our sensor can achieve 325 electrons or holes per square micrometer. Graphene nanoribbons with a lower intrinsic loss allow for less plasmon damping, giving rise to an improved detection sensitivity and resolution. As a refractive index sensor, it can achieve a sensitivity of 485 GHz/RIU. The results can facilitate applications of ultra-micro terahertz sensors.

References

[1] Nag A, Mitra A and Mukhopadhyay S C 2018 *Sens. Actuator A Phys.* **270** 177
[2] Fan C Z, Tian Y C, Ren P W and Jia W 2019 *Chin. Phys. B* **28** 76105
[3] Li J S and Chen X S 2020 *Chin. Phys. B* **29** 78703
[4] Zhang P H, Lu B Y, Sun Y W, Yu H X, Xu K X and Li D C 2019 *Biomed. Opt. Express* **10** 215
[5] Lan F, Luo F, Mazumder P, Yang Z Q, Meng L, Bao Z Q, Zhou J, Zhang Y X, Liang S X, Shi Z J, Khan A R, Zhang Z Q, Wang L Y, Yin J and Zeng H X 2019 *Biomed. Opt. Express* **10** 3789
[6] Lee S H, Choe J H, Kim C, Bae S, Kim J S, Park Q H and Seo M 2020 *Sens. Actuators B Chem.* **310** 127841
[7] Xu W D, Xie L J, Zhu J F, Tang L H, Singh R J, Wang C, Ma Y G, Chen H T and Ying Y B 2019 *Carbon* **141** 247
[8] Huang Y X, Dong X C, Liu Y X, Li L J and Chen P 2011 *J. Mater. Chem.* **21** 12358
[9] Wen D G, Bin L S, Feng Z H, Kun K X, Ming L H, Xiang L B and Yuan L S 2015 *Chin. Phys. B* **24** 118103
[10] Liu F and Cubukcu E 2013 *Phys. Rev. B* **88** 115439

[11] Kim S, Jang M S, Brar V W, Tolstova Y, Mauser K W and Atwater H A 2016 *Nat. Commun.* **7** 12323
[12] Balci S and Kocabas C 2015 *Opt. Lett.* **40** 3424
[13] Sensale-Rodriguez B, Yan R, Rafique S, Zhu M, Li W, Liang X, Gundlach D, Protasenko V, Kelly M M, Jena D, Liu L and Xing H G 2012 *Nano Lett.* **12** 4518
[14] Qing Y M, Ma H F, Yu S and Cui T J 2019 *J. Phys. D: Appl. Phys.* **52** 15104
[15] Nuttawut K S, Xiong X, Bai P, You J B, Png C E, Wu L and Hess O 2019 *Nano Lett.* **19** 5853
[16] Törmä P and Barnes W L 2014 *Rep. Prog. Phys.* **78** 13901
[17] Chen X Y, Tian Z, Li Q, Li S X, Zhang X Q, Ouyang C M, Gu J Q, Han J G and Zhang W L 2020 *Chin. Phys. B* **68** 077803
[18] Yan X, Liang L J, Zhang Z, Yang M S, Wei D Q, Wang M, Li Y P, Lü Y Y, Zhang XF, Ding X and Yao J Q 2018 *Acta Phys. Sin.* **67** 118102 (in Chinese)
[19] Niemczyk T, Deppe F, Huebl H, Menzel E P, Hocke F, Schwarz M J, Garcia-Ripoll J J, Zueco D, Hümmer T, Solano E, Marx A and Gross R 2010 *Nat. Phys.* **6** 772
[20] Wirth Lima A J, Alves Sousa P P and Bezerra Fraga W 2020 *Chin. Phys. B* **29** 37801
[21] Vasić B and Gajić R 2015 *Phys. Rev. Lett.* **4** 024007
[22] Zhang Z Y, Fan F, Li T F, Ji Y Y and Chang S J 2020 *Chin. Phys. B* **29** 078707
[23] Guo X, Hu H, Zhu X, Yang X and Dai Q 2017 *Nanoscale* **9** 14998
[24] Zhu W G, Xu H Q, Pan J T, Zhang S, Zheng H D, Zhong Y C, Yu J H and Chen Z 2020 *Opt. Express* **28** 25869
[25] Taleb F, Al Naib I and Koch M 2020 *Sensors* **20** 2265
[26] Chen H, Ma S H, Yan W X, Wu X M and Wang X Z 2013 *Chin. Phys. Lett.* **30** 030702
[27] Han Z H, Jiang H, Tan Z Y, Cao J C and Cai Y J 2020 *Chin. Phys. B* **29** 084209